

# Dynamics of Polymer Interdiffusion: The Ripple Experiment

K. A. Welp and R. P. Wool\*

Department of Chemical Engineering, and Center for Composite Materials, University of Delaware, Newark, Delaware 19716-3144

S. K. Satija

Center for Neutron Research, National Institute of Standards and Technology, Gaithersburg, Maryland 20899

S. Pispas and J. Mays

Department of Chemistry, University of Alabama at Birmingham, Birmingham, Alabama 35294

Received November 17, 1997; Revised Manuscript Received May 6, 1998

**ABSTRACT:** We explore the interdiffusion of oppositely labeled triblock polystyrene chains, HDH/DHD, during welding in the melt using dynamic secondary ion mass spectroscopy (DSIMS) and specular neutron reflectivity (SNR). The HDH chains have the central portion of the chain deuterated (D) ~50% while the two ends (H) each have ~25% protonation; the DHD is oppositely labeled, but each set of chains contains about 50% deuteration. During welding, the deuterium depth profile exhibits “ripples” whose characteristic features, such as the time and molecular weight dependent shape, amplitude, and position, are very sensitive to the microscopic details of the polymer dynamics. The ripple experiment is especially sensitive to the presence, or absence, of topological constraints and anisotropic motion of chains. The current work significantly extends the molecular weight range up to 400 000. This allows greater separation of the six key ripple features used in deciphering the correct polymer dynamics model at the polymer–polymer interface. The DSIMS and SNR experimental results are compared to theoretical predictions and ripple simulations for Rouse, polymer mode-coupling, reptation (with and without tube broadening), and other phenomenological dynamics models. The six ripple characteristics were found to be perfectly correlated and convincingly consistent with the predictions of the reptation dynamics model. The ripple results are in significant disagreement with the polymer mode-coupling model proposed by Schweizer and other tubeless models. We conclude that the reptation model, proposed by DeGennes in 1971 with parallel developments by Edwards, is the correct model to describe the dynamics of polymer interdiffusion.

## 1. Introduction

Understanding the dynamics of polymer chains at interfaces is critical to many applications, including welding, fracture strength development, composite lamination, particle sintering, coatings, adhesion, and friction.<sup>1</sup> Much work has been done on steady state or long time diffusion in polymers,<sup>2–5</sup> but it is the short time interdiffusion at a polymer–polymer interface that determines the critical properties of the interface. Short time scale is defined by motions resulting in penetration depths on the order of the radius of gyration,  $R_g$ , about 175 Å for the 400K polystyrene used in this study.

Through the use of specially labeled polymer chains, the short-range dynamics of polymers at a polymer–polymer interface can be monitored.<sup>6–8</sup> The labeling scheme is depicted in Figure 1. In each chain, roughly 50% of the total monomers have the hydrogen moieties replaced by deuterium. Thin layers comprised of chains with either the center portion labeled (HDH) or the ends labeled (DHD) are placed on opposing sides of an interface. Since the motion of the chain ends is preferred over the centers, upon welding ( $T > T_g$ ), we see an enrichment of the deuterium concentration level on the HDH side, and depletion on the DHD side of the polymer–polymer interface. On the basis of the characteristic concentration profile produced, Figure 2, this system has been called the “ripple experiment”.<sup>6–8</sup> Upon further annealing, the shape of the concentration profile changes. As shown in Figure 3, the peak height,

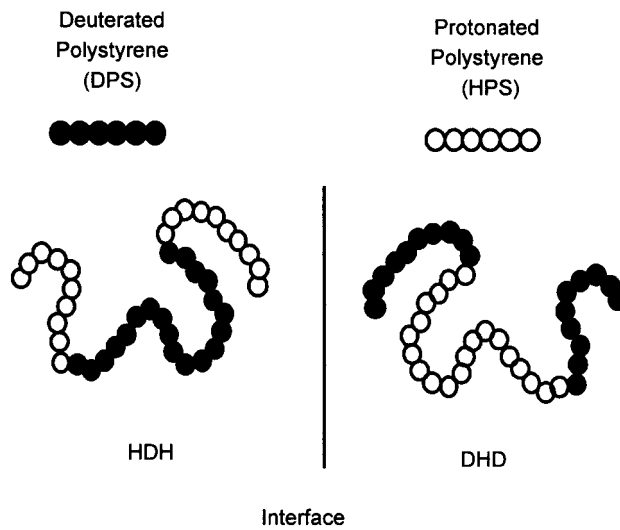


**Figure 1.** Specially labeled HDH/DHD polystyrene chains. Both chains contain 50% deuterated (D) monomers: the HDH chain has the deuterated monomers in the center of the chain, while the DHD chain has 25% of the length deuterated at each end.

$H(t)$ , peak position,  $Z_p(t)$ , and area under peak,  $A(t)$ , characterize the changes in shape of the ripple. Unique values and trends for these features are predicted for different dynamics models. Comparison of these model predictions to experimental profiles determines the

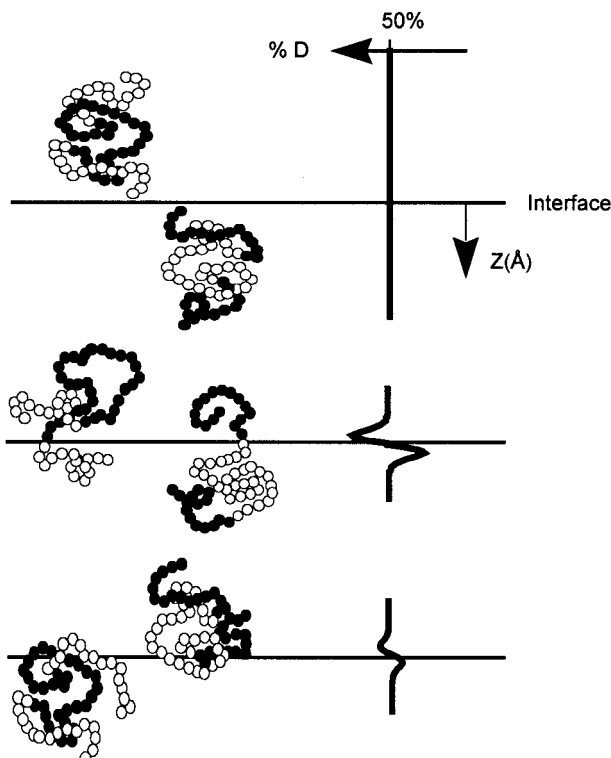


**Figure 2.** Development of a “Ripple” via enrichment/depletion in the deuterium concentration depth profile during interdiffusion of matching triblock HDH/DHD chains.

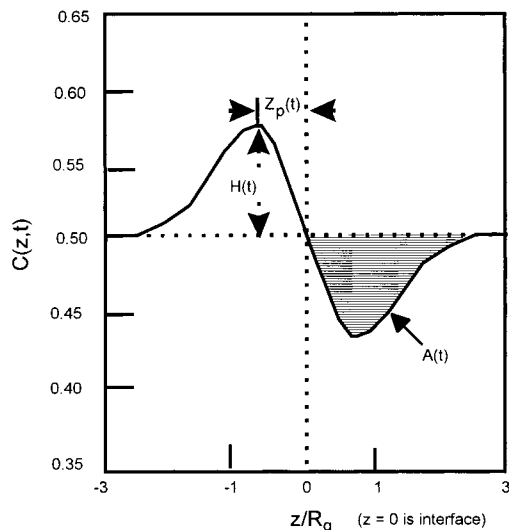


**Figure 3.** General “Ripple” profile with characteristic features, peak height,  $H(t)$ , peak area,  $A(t)$ , and peak position  $Z_p(t)$ .

correct polymer dynamics model for describing welding at the polymer–polymer interface. Specific model predictions will be discussed in section 3. Predicted values for the ripple characteristics become more separated with increasing molecular weight for different models. Prior work on these systems<sup>6–8</sup> included polymers up to 230K. The work presented here uses 400K triblock polystyrene materials, which ensures a fully entangled system with significant separation of model predictions for the characteristic features of the ripple.

To study the dynamics of polymer chains at the polymer–polymer interface requires techniques capable of penetrating through the polymer to the buried interface. High depth resolution is required to make

**Table 1. Properties of Triblock Polystyrene Materials Used in This Work**

sample	$M_w$	N	PDI	% D (mol %)
HDH	413 000	3815	1.04	55
DHD	453 000	3838	1.05	47

meaningful comparisons to model predictions. Neutron reflectivity is a very high-resolution technique ( $\sim 10 \text{ \AA}$ ) capable of penetration of several hundred angstroms; however, it is limited by the nonuniqueness of the concentration profiles derived. Dynamic secondary ion mass spectroscopy (DSIMS) is a lower resolution technique ( $\sim 50 \text{ \AA}$ ) but generates real space depth profiles with minimal data manipulation. The results presented here are obtained using both techniques. The combined DSIMS–SNR ripple experiment exploits a complementary relationship by offering high depth resolution while maintaining the confidence of real space depth profiles. The chemical design of the chains, combined with the experimental techniques to examine welding at the HDH/DHD interface, will be shown to produce convincing and conclusive results for the correct dynamics model for polymer interdiffusion.

## 2. Experimental Methods

**2.1. Sample Preparation.** Triblock poly(styrenes) were prepared using “living” anionic polymerization initiated with *sec*-butyllithium. Sequential addition of monomers produced symmetric diblock polymers. These diblocks were then coupled using dichlorodimethylsilane. If the order of monomer addition is changed, the labeling can be reversed. Care must be taken to allow preparation of high molecular weight materials.<sup>6</sup> Properties of the polystyrene triblock materials used in this work are given in Table 1. The data shown in section 4 and those of Table 1 show a slight mismatch in the levels of deuteration between HDH and DHD polymers. This initial mismatch is small, about 8%, and is difficult to remove completely in the synthesis.

Polymer bilayers were prepared on single-crystal silicon wafers (4 in. diameter, one side polished) by spin coating (Headway Research PM101DT-R790). All steps were conducted in a vertical laminar flow hood to prevent contamination. Si wafers were first degreased with acetone and toluene. Subsequently they were etched in a 7:1 buffered oxide etch (ammonium fluoride:hydrofluoric acid) (Baker) until the surface became hydrophobic and stabilized in  $\text{NH}_4\text{F}$  solution (40% weight) (Baker). The substrate was then rinsed in  $18 \text{ M}\Omega \text{ cm}$  water and spun dry with toluene. The HDH polymer, dissolved in toluene, was then spun onto the substrate. Concentrations of polymer in solution and spin speed were selected to produce films  $\sim 800 \text{ \AA}$  thick. This thickness is greater than  $4R_g$  for 400K polystyrene. The HDH (on Si) films were annealed at  $120^\circ\text{C}$  under vacuum for 12 h to remove solvent and relieve residual stress in the film.

DHD layers were prepared by spin coating onto cleaned glass slides ( $50 \times 70 \text{ mm}$ , Corning). DHD layers on glass were transferred by floating the films onto a pool of clean ( $18 \text{ M}\Omega \text{ cm}$ ) water and recovering them on the HDH coated silicon. A freshwater bath was used for each film to prevent contamination. The resulting Si/HDH/DHD samples were dried in a vacuum for 24 h at  $70^\circ\text{C}$  to remove residual water.

**2.2. Welding.** HDH/DHD bilayers were subjected to annealing at  $131^\circ\text{C}$  for differing times to produce samples with a range of interdiffusion conditions. The longest relaxation time for this material,  $\tau_d$ , is essentially the time required to diffuse a distance on the order of the radius of gyration, and was approximated by

$$\tau_d = \frac{R^2}{3\pi^2 D} \quad (1)$$

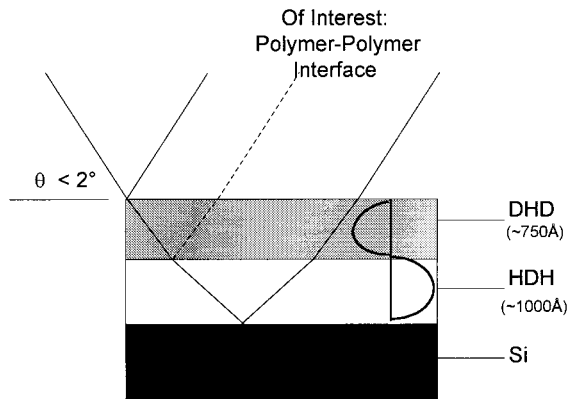


**Figure 4.** Low-angle specular neutron reflection (SNR) configuration for the DHD/HDH/Si welding experiment. A “ripple” is also sketched for reference.

Here  $R$  is the root-mean-square end-to-end distance of the chain, 427 Å for 400K polystyrene, and  $D$  is the center of mass diffusion coefficient at the steady state. The exact relaxation time, or the need to predetermine the relaxation time, is not critical to the analysis and can be deduced from the ripple experiment in an internally consistent manner. However, eq 1 was found to be useful for experimental design purposes.

The self-diffusion coefficient,  $D$ , is estimated by the Vogel relationship

$$\log(D/T) = A - B/(T - T_{\text{inf}}) \quad (2)$$

The parameters  $A = -9.789$  and  $B = 710$  are estimated from bulk diffusion data on PS at MW = 255K and  $T_{\text{inf}} = 322$  K, as obtained by Green and Kramer.<sup>2</sup> These values are used to calculate  $D(255\text{K}, T)$ , the self-diffusion coefficient at MW = 255K and the annealing temperature  $T$ . Using the scaling law,  $D \sim M^{-2}$ , the value is scaled to the molecular weight of interest, 400K. The relaxation time at 131 °C, was found to be  $\tau_d = 187$  min, approximately, which provided ample time for successive welding treatments with minimal time errors associated with cooling/heating near  $T_g$ .

**2.3. Specular Neutron Reflectivity, SNR.** Specular neutron reflectivity, SNR, experiments were performed on the NG-7 spectrometer at the NIST Center for Neutron Research (NCNR). Neutron reflectivity directs a collimated beam of neutrons onto a surface at a glancing angle (<3°) and measures the ratio of the reflected to incident intensity as a function of momentum transfer  $q_z$ , perpendicular to the interface. A schematic representation of an SNR experiment on a HDH/DHD bilayer is shown in Figure 4. The neutron momentum is determined by

$$q_z = \frac{4\pi(\sin \theta)}{\lambda} \quad (3)$$

where  $\lambda$  is the wavelength of the neutron beam and  $\theta$  the angle of incidence. The incident neutrons can be reflected or transmitted and the superposition of reflected beams from different interfaces produces the characteristic “beating” of constructive and destructive interference vs path length, which constitutes the reflection profile (Figure 5). Neutron reflection occurs due to differences in the scattering length density,  $\rho_b$ , which is analogous to reflection of visible light or X-rays from materials with differences in index of refraction or electron density, respectively. The H- and D-segments of the HDH and DHD samples have high contrast, as evidenced by the  $\rho_b$  values for the species in the system,  $6.3 \times 10^{-6}$  Å<sup>-2</sup> for deuterated polystyrene,  $1.4 \times 10^{-6}$  Å<sup>-2</sup> for protonated polystyrene, and  $2.1 \times 10^{-6}$  Å<sup>-2</sup> for silicon. Detailed treatments of reflectivity appear in the literature.<sup>1,9-11</sup>

The concentration depth profiles were obtained from the neutron reflectivity data by a new fitting process. To optimize and improve the fitting routine, a series of functions were

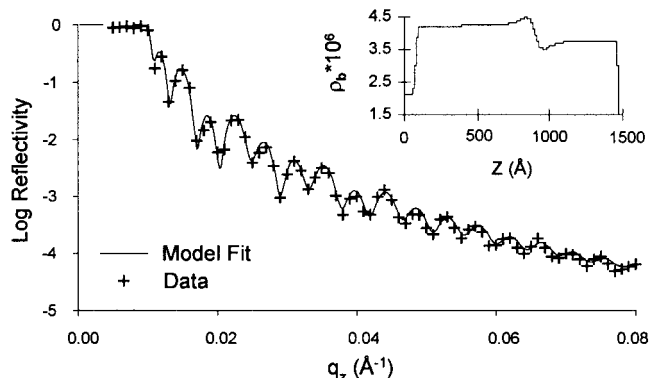


**Figure 5.** Log of the reflectivity vs neutron momentum for the 400K DHD/HDH/Si sample at an annealing time of  $0.14\tau_d$ . The solid curve through the experimental points is calculated from the model scattering length density,  $\rho_b$ , vs depth profile for the Ripple, shown as an inset.

prepared, based on the literature,<sup>12</sup> that allow the fitting to be performed within a convenient Excel spreadsheet environment.<sup>13</sup> The new approach combines simultaneous numerical and graphical data interactively, with command-free calculation updates, to improve the flexibility and speed of the fitting procedure. The new approach, entitled SERF<sup>13</sup> (spreadsheet environment reflectivity fitting) has been analyzed in detail with respect to known depth profiles and compared with state-of-the-art reflectivity fitting techniques. For example, Figure 5 illustrates a typical reflectivity curve for the 400K DHD/HDH/Si samples described above. The calculated model scattering length density profile for the ripple, as obtained by the SERF method, is shown as an inset in Figure 5. The “goodness of fit” is determined by the model depth profile’s ability to back-calculate the actual experimental data, as shown by the solid line through the experimental points. Optimization of the fitting parameters is done quantitatively using the SERF method, and convergence is achieved in a complementary manner with user judgment via instantaneous graphical feedback.

**2.4. Dynamic Secondary Ion Mass Spectroscopy, DSIMS.** Dynamic secondary ion mass spectroscopy (DSIMS) measurements were performed at the Center for Microanalysis of Materials, University of Illinois at Urbana-Champaign, on a Cameca IMS-5f instrument. DSIMS involves the sputtering of a surface by repeatedly scanning a high energy ion beam over a given area and measuring ejected ionized molecular fragments in a mass spectrometer. The ion beam effectively shaves-off a thin layer of material (~20 Å) on each scanning cycle and the analysis of the ion fragments, or secondary ions, from successive layers in the crater provides a method of depth profiling through a buried interface. The depth resolution (~50 Å) is determined by the “knock-on” ballistic damage done by the ion beam fragmentation process. Figure 6 shows a schematic of the DSIMS experiment on a DHD/HDH bilayer on a silicon substrate. The concentration profile of deuterium, hydrogen, and carbon is obtained by monitoring the secondary ion current, for the appropriate atomic mass, in the material ejected from the crater. Detailed descriptions of the DSIMS method appear in the literature.<sup>1,14-17</sup>

In the ripple experiments, a Cs<sup>+</sup> primary ion beam (14.5 keV, 25 nA) was used to sputter through the interface. The Cs<sup>+</sup> beam was selected to minimize ballistic penetration, reduce knock-on damage, and improve resolution, compared to other ion beams. The beam was rastered over a crater 175 × 175 mm and the average sputtering rate was 0.47 Å/s. Secondary ions were produced over the entire surface of the crater, but mechanical gating was used to select those from a circular region of diameter 10 μm in the center of the crater and, hence, eliminate crater-edge sputtering effects. The latter can significantly lower depth resolution.

Annealed HDH/DHD samples were coated with gold (~200 Å) to allow conduction of the charge buildup generated in the

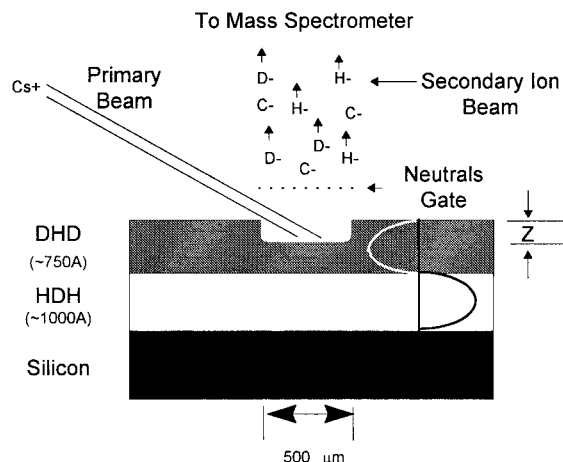


**Figure 6.** Dynamic secondary ion mass spectrometry (DSIMS) experiment for the DHD/HDH bilayer on a Si substrate. A “ripple” is sketched for reference.

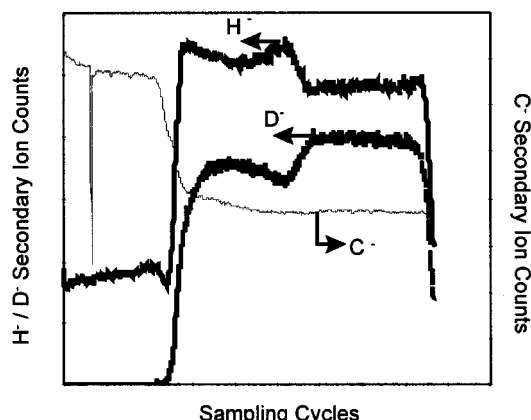


**Figure 7.** Typical raw data from a DSIMS experiment showing the secondary ion count vs sampling cycles (depth) on the 400K HDH/DHD bilayer, at an annealing time of  $0.25\tau_d$ . The ripple is clearly evident in both the  $\text{D}^-$  and  $\text{H}^-$  signals. The plateau region of the  $\text{C}^-$  signal indicates the presence of polymer at a constant sputtering rate, allowing conversion of the cycle time axis to depth via the known bilayer thickness, as determined by ellipsometry.

sputtering process. In addition, an electron flood gun was used to neutralize any positive charge accumulation that would adversely affect the yield of negative ions detected by the mass spectrometer. Due to the uncertain concentration of water vapor in the sample chamber and its continuous removal by the vacuum system during scanning, there is some uncertainty in the  $\text{H}^-$  signal,<sup>14,15</sup> and therefore, all significant quantitative data interpretation was done using the  $\text{D}^-$  signal.

Figure 7 shows typical raw DSIMS data for the HDH/DHD ripple experiment, where the secondary ion count vs sputtering time (related to depth), is plotted for individual  $\text{H}^-$ ,  $\text{D}^-$ , and  $\text{C}^-$  ions. Assuming a constant sputtering rate through the polymer layers, identified by monitoring a constant  $\text{C}^-$  signal common to both layers, the time axis was converted to distance via the known polymer bilayer thickness. The thickness is measured by ellipsometry prior to Au coating. The  $\text{D}^-$  secondary ion counts vs distance profiles were then used to measure ripple characteristics, as outlined in Figure 3. Characteristic features of the profile were read from the DHD side (top layer) of the “ripple”, as sample damage builds up with increasing sputtering depth, thus lowering resolution. Concentration profile characteristics were normalized by the baseline to account for variations from sample to sample, as well as allowing comparison to dynamics predictions. The Ripple characteristics were derived as follows: the peak height,  $\bar{H}(t)$ , was determined by the difference between the extremum and the baseline values, normalized by the baseline; the peak area,

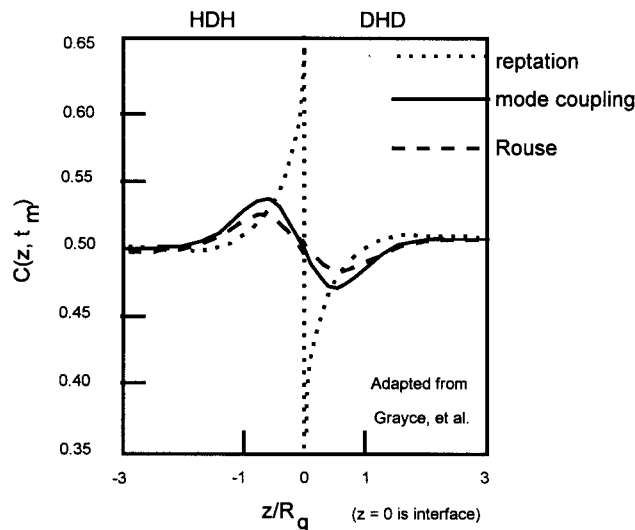


**Figure 8.** Model predictions for the ripple deuterium concentration depth profiles at their maximum amplitudes and welding time  $t_m$ , for reptation ( $d = 0$ ), polymer mode-coupling (PMC), and Rouse dynamics.

$A(t)$ , is the region between the baseline value and the secondary ion trace, again normalized by the baseline value; the peak position,  $Z_p(t)$ , is the distance of the peak position from the interface, and the interface position ( $z = 0$ ) is determined by the inflection point of the secondary ion count trace. Since the DSIMS method is destructive, a series of samples was prepared and welded for appropriate times, such that each sample provided one data point vs welding time.

### 3. Dynamics Model Predictions

All polymer dynamics models predict ripple profiles for interdiffusion of oppositely labeled triblocks (HDH/DHD). The predicted ripple characteristics ( $H$ ,  $A$ ,  $Z_p$  in Figure 3) are significantly different and allow conclusions to be made about the correct dynamics model for polymer interdiffusion. During the course of welding, the ripple height will go through a maximum value,  $H_{\max}$ . The time at which this maximum is reached is  $t_m$ . The area under one peak of the ripple at any time, is designated as  $A(t)$ , while  $A_{\max}$  designates the area at  $t_m$ . The distance of the peak from the interface along the depth axis is the peak position,  $Z_p(t, M)$ . The dependence of the peak position on welding time and molecular weight proves to be critical in differentiating between important dynamics model candidates presented in the following sections.

Model Ripple calculations for Rouse,<sup>18</sup> polymer mode-coupling (PMC),<sup>19</sup> and reptation<sup>20,21</sup> dynamics have appeared in the literature.<sup>22</sup> These data (Figure 8), in addition to simulation and calculation work done by the authors,<sup>1,6,23</sup> are discussed in the following sections.

**3.1. Rouse Dynamics.** The Rouse model<sup>18</sup> was not originally intended for highly entangled melt dynamics and thus is not expected to apply, except for short segmental lengths of order of the entanglement spacing. However, it appears as the dynamics kernel in nearly all models and provides an excellent basis for model comparison. The Rouse model, consisting of  $N$  beads attached by  $N - 1$  springs, is used here as an important default case for behavior representing isotropic monomer friction coefficients and where anisotropic motion occurs only via bead-bead connectivity. The Rouse model represents the Brownian motion of a Gaussian chain in an unstructured medium that serves as the hot

**Table 2. Dynamics Model Predictions for Ripple Characteristics, Maximum Ripple Amplitude,  $H_{\max}$ , Area at Maximum Amplitude,  $A_{\max}$ , Peak Position at Maximum Amplitude,  $Z_p(t_m)$ , Time of Maximum Amplitude,  $t_m$ , Time and Molecular Weight Dependencies of Peak Position, from Various Polymer Dynamics Models**

400K	Reptation		Reptation		TAC
HDH/DHD	Rouse	PMC	( $d = 0$ )	( $d \neq 0$ )	
$H_{\max}$ (%)	5.4	7.0	21.8	11.0	$\approx 10-15$
$A_{\max}$ (Å)	8.8	11.7	15.0	14.5	$\approx 15$
$Z_p(t_m)$ (Å)	122	114	0.0	60 ( $\approx d$ )	$\approx R_g$ (ends)
$t_m/\tau$	0.5	0.58	0.25	0.25	$\approx 0.25$
$Z_p(t) \sim t^\alpha$	$\alpha \sim 1/4$	$\alpha \sim 1/4$	$\alpha = 0$	$\alpha = 0$	$\alpha > 0$
$Z_p(t_m) \sim M^\beta$	$\beta = 1/2$	$\beta = 1/2$	$\beta = 0$	$\beta = 0$	$\beta > 0$

bath. With the HDH/DHD interface, the increased mobility of the chain ends results in a ripple that shows enrichment on the HDH side and depletion on the DHD side of the interface, as shown in Figure 8. The ripple characteristics for the Rouse model are summarized in Table 2 and behave as follows:

The peak height,  $H(t)$ , increases, reaches a maximum value and then decays away as the chain centers begin to catch up with the ends. The peak height maximum,  $H_{\max}$ , of about 5.4%, occurs at a depth of about  $0.7R_g$ , or 122 Å for the 400K sample. Since both the chain ends and centers are interdiffusing together, the peak height, reflecting differences between chain end and center motion, is relatively small.

The area under the peak,  $A(t)$ , behaves in a manner similar to the height, increasing, passing through a maximum, and then decaying. The area at the maximum height,  $A_{\max}$ ,  $\approx H_{\max}R_g$ , is about 8.8 Å.

The peak position,  $Z_p(t)$ , for the Rouse model propagates away from the interface continuously as welding progresses and is expected to behave as  $Z_p(t) \sim t^\alpha$ , with  $\alpha \approx 1/4$ .

The  $Z_p$  propagation behavior is highly characteristic of nontube dynamics models. At the peak height  $H_{\max}$ , the peak position  $Z_p(t_m)$ , is located about  $0.7R_g$  away from the interface. The peak depth position is seen in these calculations to scale with  $R_g$ , and thus,  $Z_p(t_m, M) \sim M^\beta$ , with  $\beta = 1/2$ . The predictions of the Rouse model are summarized in Table 2.

**3.2. Polymer Mode-Coupling Dynamics.** The polymer mode-coupling model of Schweizer<sup>19</sup> equates the motion of a single polymer in the bulk to the Brownian motion of a Gaussian chain, similar to the Rouse model. However, while the friction coefficient for the Rouse model is effectively constant, in the PMC model the friction coefficient for each bead, though isotropic, is determined by a memory function which depends on the current and past trajectories of all the other beads. This model is important in that no *a priori* assumptions are made about tubes, entanglement constraints, etc. The model is developed from statistical mechanics and requires only independently measurable parameters as inputs. The behavior of the PMC ripple, Figure 8, is similar to that of the Rouse model, but with slightly higher  $H_{\max}$  and  $A_{\max}$  values, as shown in Table 2. The coupling of the dynamics of various chains extends the time scale of the motions, resulting in a larger  $t_m$ , but the peak shape and position behaviors as a function of time and molecular weight are very similar to the Rouse model predictions.

**3.3. Reptation Dynamics.** De Gennes<sup>20</sup> introduced the reptation model in 1971, with parallel developments from Doi and Edwards,<sup>21</sup> to model a chain diffusing in a gel or network with a characteristic entanglement

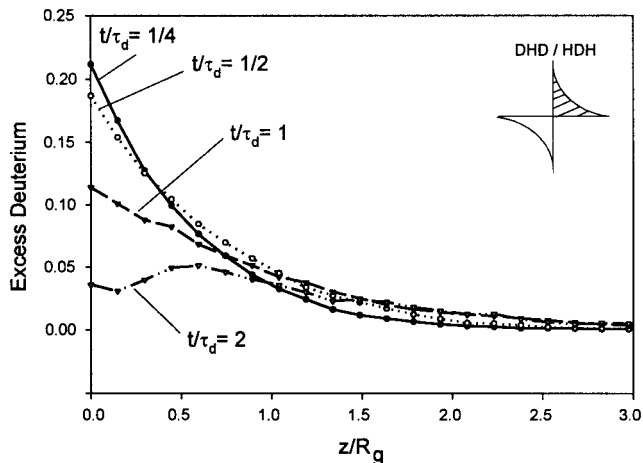


**Figure 9.** A quadrant of the ripple concentration vs depth ( $z/R_g$ ) profiles obtained from the reptation model computer simulations ( $d = 0$ ) for welding times  $t$ , normalized with respect to the reptation time,  $\tau_d$ . The Ripple peak reaches a maximum height  $H_{\max}$ , near  $t/\tau_d = 1/4$  and the peak position  $Z_p(t) \sim t^\alpha$  remains at the interface plane  $z/R_g = 0$ , up to  $t/\tau_d = 1$ . Further annealing at  $t/\tau_d > 1$  causes the peak position to propagate away from the interface toward  $z/R_g \sim 1$ . At  $t/\tau_d = 2$ , a low amplitude ripple is observed near  $Z_p = 0.5R_g$  which is comparable in magnitude and shape to the Rouse or PMC ripples.

spacing  $M_e$ . A single chain is viewed as moving coherently back and forth in a tube of topological constraints (diameter =  $d$ ). This model is fundamentally different from the Rouse and PMC models with respect to the highly anisotropic, snakelike, nature of the motion. Figure 8 shows the result of numerical calculations using the reptation model with a zero diameter tube (maximum anisotropy) performed by Grayce et al.<sup>22</sup>

Reptation ripples were generated using computer simulation on a two-dimensional lattice. Random walk chains were formed at varying distances from a reflecting boundary condition surface. Chain motions were induced by random selection of an end bead and addition of a new bead at a randomly selected adjacent lattice site, followed by removal of the end bead from the opposite end of the chain. Many chains were built and moved in succession, while important properties were calculated and averaged over all chains at the completion of a run. Scaling laws for the simulated static and dynamic properties, e.g., chain dimension, relaxation time, and bulk diffusion coefficient, were found to be in agreement with the reptation model predictions.

The ripples obtained by this reptation simulation are shown in Figure 9 and have the following characteristics: In both Figures 8 and 9 it is evident that the Reptation ripple has a much larger maximum height,  $H_{\max} \approx 22\%$ , than the PMC or Rouse predictions. The peak area  $A$ , behaves similarly, and the value at maximum height,  $A_{\max}$ , is approximately 15 Å. All ripples prior to the  $t = \tau_d$  profile in Figure 9 have a peak located on the interface, i.e.,  $Z_p(t) \approx 0$ . The ripple simulation data in Figure 9 clearly demonstrates that the peak position,  $Z_p(t)$ , is constant ( $\alpha = 0$ ) for welding times up to the relaxation time of the chains after which it begins to propagate.

The effect of Rouse motions on length scales less than the tube diameter ( $d$ ) can be accounted for in the calculation of ripples using the reptation model ( $d \neq 0$ ).<sup>22</sup> Predictions of both approaches are included in Table 2.

Lateral Rouse-like motion within the tube decreases the maximum value of the peak height. The peak position is again constant with welding time, but now is located at  $Z_p \sim d$ , the tube diameter, and not on the interface. The peak position then scales with the tube diameter, which is independent of molecular weight, and thus  $Z_p(t_m, M) \sim M^0$  and  $\beta = 0$  for the reptation model.

The ripple characteristics can be readily calculated using the minor chain reptation model of interdiffusion, developed by Kim and Wool.<sup>1,24</sup> The minor chain model tracks the relaxation of a polymer chain by following segments of the polymer chain which have escaped their initial position, or tube. There are two such segments per chain, called minor chains. The length of a minor chain grows with time, as

$$L(t) = \frac{L_0}{2} \left( \frac{t}{\tau} \right)^{1/2} \quad (4)$$

Here  $L_0$  is the total chain length, and  $\tau$  is the relaxation time of the material. The maximum height for the ripple predicted by the minor chain model is expected when  $L/L_0$  is  $1/4$  due to the triblock architecture, and from eq 4, we obtain  $t_m \approx \tau/4$ . As we have seen previously, the peak is expected at the interface (in a zero diameter tube approach); therefore  $H(t)$  equals  $C(0, t)$  for  $t < t_m$ , and we predict the Ripple peak height as

$$H(t) = \frac{1}{2} \left( \frac{t}{\tau} \right)^{1/2} \quad (t \leq t_m) \quad (5)$$

On the basis of this relation and the  $t_m$  result above, we can see that the maximum peak height,  $H_{\max}$ , predicted by the minor chain scaling relations is 25%. The area under the peak can also be predicted by the minor chain model<sup>1</sup>

$$A(t) \approx \frac{R_g}{4} \left( \frac{t}{\tau} \right)^{3/4} \quad (t \leq t_m) \quad (6)$$

The area at maximum height,  $A_{\max}$ , is then  $0.09 R_g$ , which is about 15 Å for the 400K polymer. It is evident that the results from minor chain reptation scaling relations follow the same trend as those of the numerical calculations and computer simulations discussed above. The minor chain scaling relations offer accurate and simple predictions for the molecular properties of polymer interfaces, provided the reptation model is correct.

**3.4. Other Dynamics Models.** Additional models have been proposed for polymer dynamics in the literature, and much of this work is reviewed by Lodge et al.<sup>25</sup> We can classify the majority of the available models as either tubeless or tube (modified reptation), based on the form of the friction which the models produce (isotropic or anisotropic, respectively). Some important tubeless models, in addition to the Rouse and PMC models, include the developments of Skolnick and Kolinski,<sup>26</sup> Ngai et al.,<sup>27,28</sup> and Herman.<sup>29,30</sup> Modified reptation developments include those of Hess,<sup>31</sup> Kavassalis and Noolandi,<sup>32</sup> Fixman,<sup>33,34</sup> Doi,<sup>35,36</sup> Daoud and DeGennes,<sup>37</sup> desClouzoix,<sup>38,39</sup> and Graessley,<sup>40</sup> as well as others. In addition to these examples, an important tubeless phenomenological model was brought to our attention and will be discussed in section 3.4.1. Finally, hairpin models (discussed in section 3.4.2) are based on the presumption that the motion of chain loops predominates over that of the chain ends, and they produce

results significantly different from those of all other models in the ripple experiment.

**3.4.1. Tubeless Anisotropic Coefficient Model, TAC.** It has been suggested that an isotropic friction coefficient may not be appropriate for polymers near an interface.<sup>6</sup> If instead a friction coefficient that changes along the length of the chain as a function of monomer displacement is used in a tubeless model, the anisotropy inherent in the assumptions of the reptation model may be introduced without invoking the concept of a tube. This "thought" model has been called the "tubeless anisotropic friction coefficient" or TAC model. The model states that if the mean square distance from a monomer to the nearest end of the chain is less than the mean square monomer displacement for the entire chain,  $g(t)$ , then the monomer has motions large enough to move around self-entanglements resulting from the nonequilibrium conformations of the surface chains. Therefore, the motion of a monomer satisfying this condition is considered not entangled, and has an isotropic friction coefficient. Alternatively, a monomer whose mean square displacement to the nearest chain end is greater than  $g(t)$  cannot, in general, move beyond the self-entanglements in a time  $t$ . These monomers are then constrained to move only where the chains surrounding them allow. If the component of the friction coefficient in a given direction is set proportional to the density of monomers which started on the same side of the interface in that direction, the result will potentially be an anisotropic friction coefficient for these monomers. The number of monomers that experience this anisotropic friction is determined by the magnitude of  $g(t)$ , and thus the degree of anisotropy is time dependent. No mechanism of motion is assumed other than the presence of the anisotropic entanglement constraints.

The ripple produced by this model may be similar in some respects to that predicted by the reptation model at short times, comparable to the Rouse entanglement relaxation time, but should be readily distinguishable at times less than the relaxation time. The maximum amplitude is reached approximately when  $g(t)$  reaches the mean square distance from the chain end to the junction point of the protonated and deuterated segments. This would occur near  $t_m$  seen for the reptation model.  $Z_p$  is expected to begin propagating after diffusion distances on the order of the radius of gyration for the end section of the chain,  $R_g(\text{ends})$ . This results in a peak position that is stationary at short times, but begins to move away from the interface earlier than the reptation prediction. While no exact quantitative or simulation treatment of the TAC model exists, one could conjecture that  $H_{\max}$  and  $A_{\max}$  should be slightly less than the reptation prediction due to the higher probability of center monomers crossing the interface, but still significantly larger than the purely isotropic friction models. For high molecular weight polymers, the self-entanglements due to reflecting boundary conditions on the chains near the surfaces will be relaxed as diffusion commences and the TAC ripple peaks will begin to propagate, similar to the Rouse and PMC models.

**3.4.2. Hairpin.** Hairpin models have been suggested<sup>26,29,30</sup> where the segments of the chain away from the ends can move laterally to the chain contour. This is the motion expected for the diffusion of ring polymers. The use of hairpin models for linear chains is motivated by the fact that high molecular weight chains have

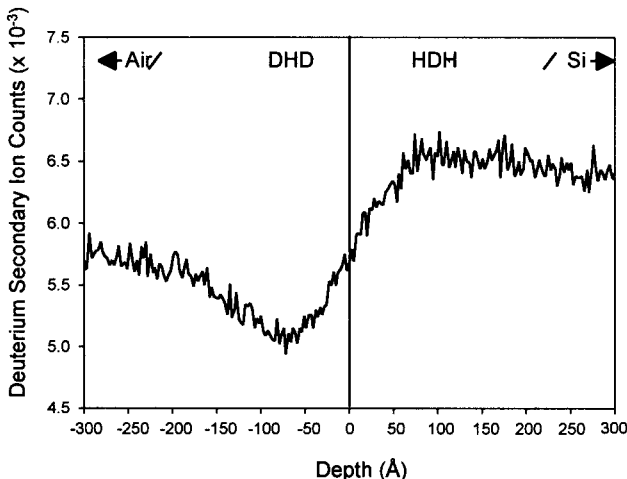


**Figure 10.** Ripple profile,  $D^-$  ion counts vs depth, obtained from the DSIMS experiment at  $t = 0.38 \tau_d$ , for the DHD/HDH interface. The secondary ion counts axis has not been scaled. The  $D^-$  depletion on the DHD side results from the migration of the  $D^-$  chain ends to the HDH side.

many more loops than ends. The energy for a loop to propagate is much higher than an end, but the models theorize that the number of loops is sufficient for this motion to dominate. Since this model predicts that the motion of the chain centers is faster than that of the ends, the ripple shape should be inverted compared to other predictions, enriched on the DHD side, and depleted on the HDH side. The ends should also have a high probability of motion, and thus the Ripple is likely to wash out completely in a detailed treatment of the model. Additionally, the concurrent motion of centers and ends, such as Rouse and PMC, gives an increasing  $Z_p(t)$ , as summarized in Table 2.

#### 4. Results and Discussion

**4.1. Experimental Results. 4.1.1. Dynamic Secondary Ion Mass Spectroscopy Results.** HDH/DHD bilayer samples were welded for times up to, and beyond, the longest relaxation time of the material,  $\tau_d$ . DSIMS and SNR were used to measure deuterium profiles at each welding time to determine the behavior of the ripple. Figure 10 shows the results of a DSIMS scan after welding for  $0.38\tau_d$ . The ripple is clearly evident: the peak height,  $H(0.38\tau_d) \approx 6\%$  and the area  $A(0.38\tau_d) \approx 15 \text{ \AA}$ . The peak position is the easiest Ripple feature to determine from Figure 10, and clearly,  $Z_p \approx 70 \text{ \AA}$ .

The change in the (DSIMS) peak height with welding time is shown in Figure 11 for a sequence of samples. The height passes through a maximum of  $H_{\max} \approx 11\%$  near  $t_m \approx \tau_d$ . The progression of the (DSIMS) peak area with welding time is shown in Figure 12 and shows an  $A_{\max}$  value of approximately  $16 \text{ \AA}$ . The DSIMS data show a peak position that remains constant (Figure 13) for welding times less than the relaxation time and then begins to move away from the interface at the relaxation time.

**4.1.2. Specular Neutron Reflectivity Results.** Figure 14 shows (a) the progression of reflectivity profiles for a bilayer sample at progressively longer welding times and (b) the corresponding ripple profiles. The reflectivity curves are offset vertically for clarity, and normalized welding times are noted at the right. Changes in the reflectivity are evident in the middle of

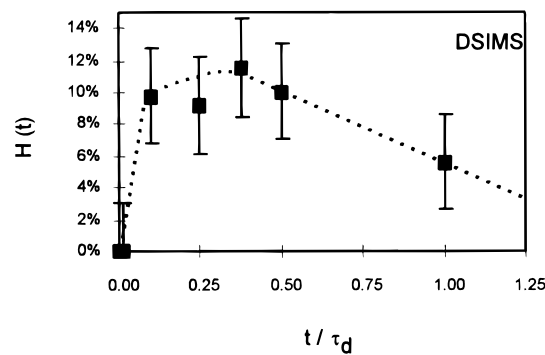


**Figure 11.** The normalized (DSIMS) peak height,  $H(t)$ , vs welding time  $t/\tau_d$  for the 400K HDH/DHD bilayers, welded at  $131^\circ\text{C}$  for the times indicated ( $\tau_d = 187$  min). Each point represents a separate bilayer. The dashed curve is sketched for illustrative purposes only.

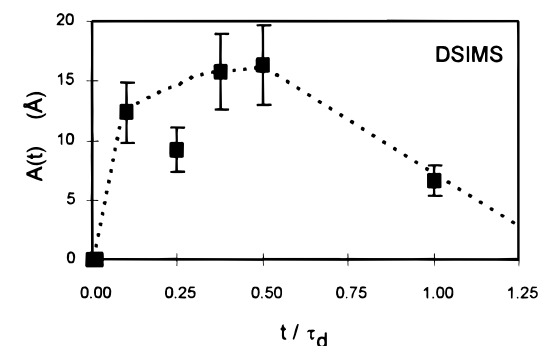


**Figure 12.** The normalized (DSIMS) ripple area,  $A(t)$ , vs  $t/\tau_d$  for the 400K HDH/DHD bilayer, welded at  $131^\circ\text{C}$  for the times indicated ( $\tau_d = 187$  min). The curve is sketched for illustrative purposes only.

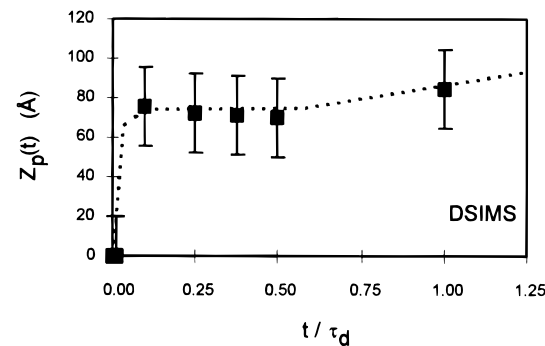


**Figure 13.** The (DSIMS) peak position,  $Z_p(t)$ , vs  $t/\tau_d$  for the 400K HDH/DHD bilayer, welded at  $131^\circ\text{C}$  for the times indicated ( $\tau_d = 187$  min.). The curve is sketched for illustrative purposes only. Note that  $Z_p(t) \sim t^0$  for  $t/\tau_d < 1$ .

the  $q_z$  range, corresponding to significant changes in the deuterium depth profile. The SERF fitting method was used to obtain ripple depth profiles from the reflectivity data. Figure 14b shows a section of the resulting scattering length density curves, converted to deuterium fraction and plotted vs depth. Initially, at  $t/\tau_d = 0$ , the slight mismatch in deuterium content between the HDH and DHD polymers is evident. The Ripple appears rapidly above this mismatch level and persists at high amplitude to  $1/2 \tau_d$ . At the relaxation time of the material,  $t/\tau_d = 1$ , the Ripple has decreased in amplitude, but the distance of the peak from the interface plane  $Z_p$  shows little change, similar to the DSIMS result in Figure 13.

The progression of peak height with welding for the SNR experiments is highlighted in Figure 15 for two

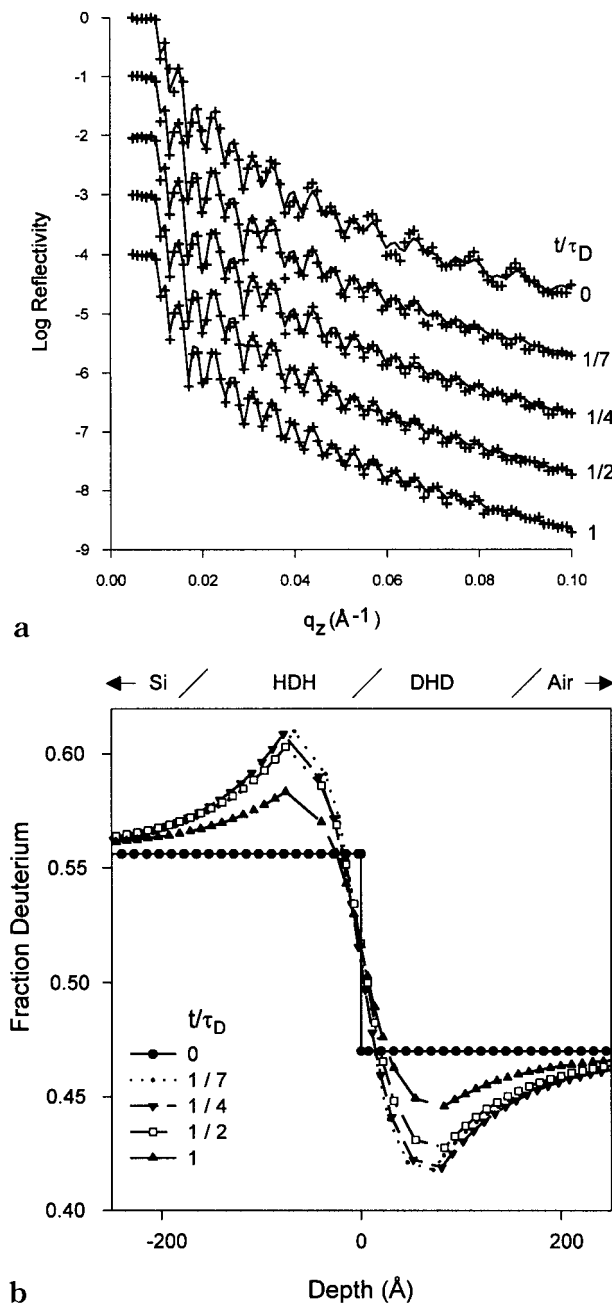


**Figure 14.** (a) A progression of (vertically offset) reflectivity profile ( $\log R$  vs  $q_z$ ) data at different welding times. Changes in the midrange of momentum transfer,  $q_z$ , can be seen. The excess deuterium fraction vs depth profiles determined from the reflectivity data above is shown at the corresponding welding times indicated in the legend. No ripple is seen initially at  $t = 0$ ; a strong ripple develops from  $t/\tau_d = 1/7$  through  $1/2$ , with a maximum amplitude near  $t/\tau_d = 1/4$ . The peak position  $Z_p(t) \sim t^0$  and remains at about 60 Å but decays away when  $t/\tau_d > 1$ .

bilayer samples. The peak height passes through a maximum,  $H_{\max}$ , of 11% near  $t/\tau_d \approx 0.25$  and decays to a value of 5–6% at  $\tau_d$ . The progression of the peak area, displayed in Figure 16, is similar to the peak height, and passes through a maximum,  $A_{\max} = 12.5$  Å at  $t_m/\tau_d = 1/4$ . Figure 17 clearly demonstrates the dependence of the peak position on welding time as,  $Z_p(t) \sim t^0$ . The peak is stationary at around 65 Å and begins to move away from the interface when the relaxation time is reached, similar to the DSIMS result. Welding beyond the longest relaxation time of the material shows a peak whose height continues to decay and a peak position

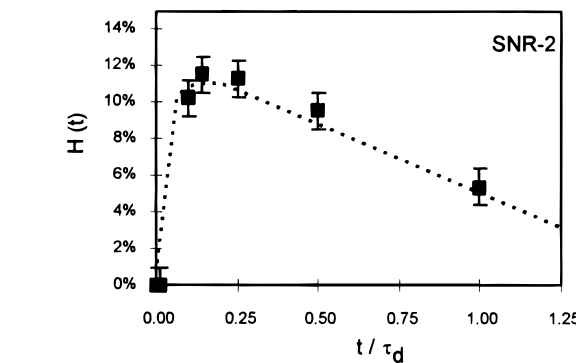
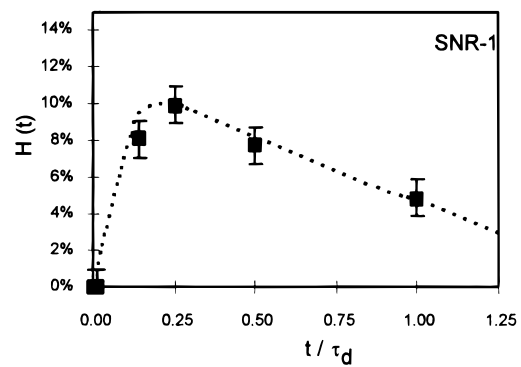


**Figure 15.** Normalized (SNR) ripple peak height,  $H(t)$ , vs  $t/\tau_d$ , for two 400K HDH/DHD bilayers, welded progressively at 131 °C for the times indicated ( $\tau_d = 187$  min). The dashed curve is sketched for illustrative purposes only.

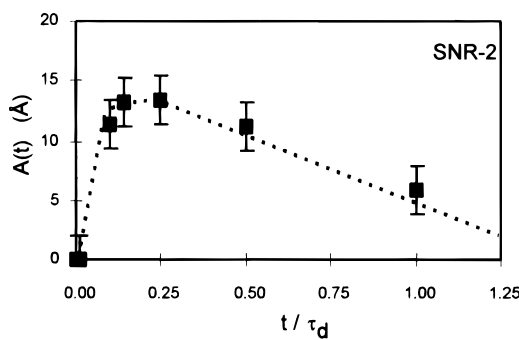
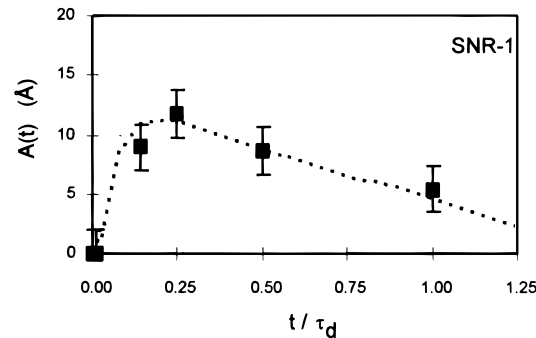


**Figure 16.** Normalized (SNR) Ripple area,  $A(t)$ , vs  $t/\tau_d$  for two 400K HDH/DHD bilayers, welded at 131 °C for the times indicated ( $\tau_d = 187$  min). The dashed curve is sketched for illustrative purposes only.

that moves away for the interface. Results in this long welding regime are hard to quantify accurately due to the decreased sensitivity of both SNR and DSIMS for broad interfaces.

Combining results for the 400K sample and those for other molecular weights,<sup>6,41</sup> the molecular weight de-

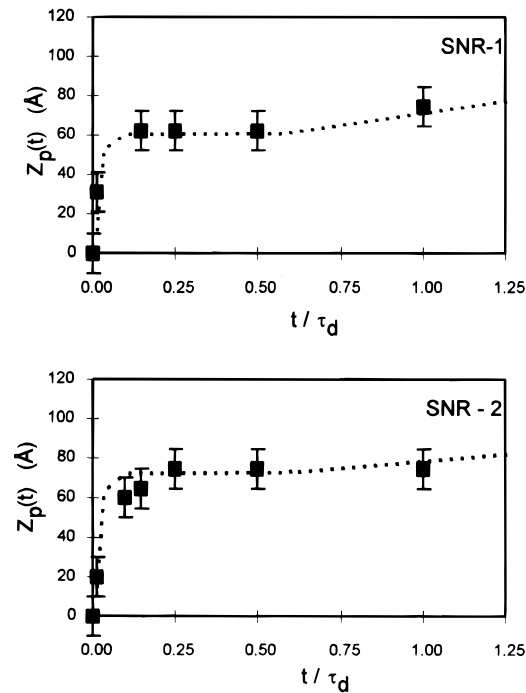


**Figure 17.** The (SNR) ripple peak position,  $Z_p(t)$ , vs  $t/\tau_d$  for the 400K HDH/DHD bilayers, welded at 131 °C for the times indicated ( $\tau_d = 187$  min). The dashed curve is sketched for illustrative purposes only.

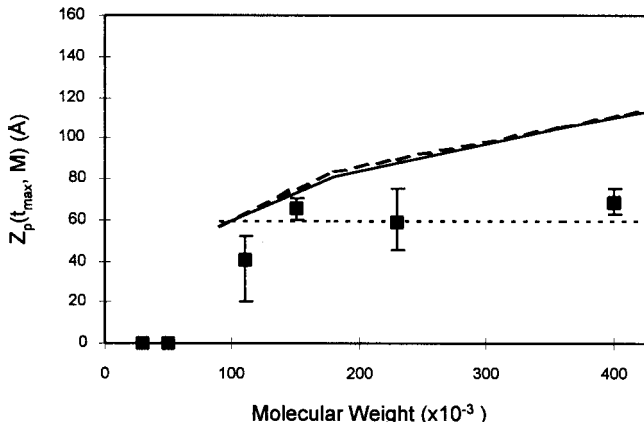


**Figure 18.** Ripple peak position at maximum amplitude,  $Z_p(M, t_m)$ , vs molecular weight. The Rouse (solid line), PMC (long dash), and reptation (horizontal dash) predictions are shown. Model predictions were derived from Grayce et al.;<sup>22</sup> some data were derived from Agrawal et al.<sup>6</sup>

pendence of the peak position,  $Z_p(t_m, M)$ , is illustrated in Figure 18. These data show that  $Z_p(t_m, M) \sim M^0$  ( $\beta = 0$ ) for all molecular weights above 110K and that no ripples are observed in the vicinity of the entanglement molecular weight (30K). Results for the ripple characteristics determined in DSIMS and SNR experiments for the 400K bilayer (HDH/DHD) samples are summarized Table 3.

**4.2. Peak Height,  $H(t)$ , Discussion.** Comparing the  $H_{\max}$  values obtained in these experiments, Table 3, to the model predictions given in section 3 and summarized in Table 2, we see reasonable agreement with the reptation ( $d \neq 0$ ) and TAC models. The DSIMS height interpretation is complicated by instrumental smearing effects, hence the large error bars shown in Figure 11. The SNR data, Figures 14b and 15, show a maximum peak height that is clearly larger than the PMC and Rouse predictions. The predictions of the TAC

**Table 3. Maximum Values of Peak Height,  $H_{\max}$ , Area,  $A_{\max}$ , Peak Position at Maximum Height,  $Z_p(t_m)$ , and Time of Maximum Amplitude,  $t_m$ , from Deuterium Depth Profiles of 400K HDH/DHD Bilayers Measured by SNR and DSIMS**

	SNR	DSIMS
$H_{\max}$ (%)	$11 \pm 1$	$11 \pm 5$
$A_{\max}$ (Å)	$12.5 \pm 2.5$	$16.3 \pm 4.2$
$Z_p(t_m)$ (Å)	$65 \pm 10$	$72 \pm 19$
$t_m$	$0.2-0.25\tau_d$	$0.15-0.35\tau_d$
$Z_p(t) \sim t^{\alpha}$	$\alpha = 0$	$\alpha = 0$
$Z_p \sim M^{\beta}$	$\beta = 0$	$\beta = 0$

model are purely qualitative, so it is difficult to discuss the model in detail. As  $t/\tau_d$  approaches 1,  $H(t)$  decreases toward 5%, which is close to the PMC and Rouse maximum height predictions  $H_{\max}$ , for these models.

**4.2.1. The Static Ripple.** It is appropriate here to discuss a “ripple” that can develop due to static considerations and the labeling scheme of the triblock chains, which we call the “static” ripple. All random coil chains have end portions that are farther from the center of mass than the center portions of the chain due to chain connectivity. It is also known that chains form distorted coils near an interface, due to the reflecting boundary condition imposed by the interface, and relax to Gaussian coils at the relaxation time of the material. If the center of mass of the chains has not moved significantly, the combination of the HDH/DHD triblock architecture and the larger distance of the end vs the center from the chain center of mass produces a small ripple. This is the static ripple, and it occurs at the relaxation time of the material and disappears with the onset of long range center of mass motions. Essentially all models should exhibit the static ripple, regardless of the dynamics. The static ripple shows peak height, area, and position values similar to those of the Rouse and PMC models, which is expected for all nontube models. The experimental results are consistent with the formation of the reptation ripple at  $t/\tau_d = 1/4$  and which then decays to the lower value of the static ripple at  $t/\tau_d = 1$ .

**4.3. Peak Area,  $A(t)$ , Discussion.** The maximum peak area  $A_{\max}$  data presented in Table 3 can be compared to the model predictions summarized in Table 2. Again the data are consistent with the reptation prediction of 14.5 Å within the uncertainty in the data. The experimental  $A_{\max}$  values are higher than those predicted by either the Rouse or PMC models. Again we see  $A(t)$  (Figures 12 and 16) tending to the Rouse and PMC predictions as  $t/\tau_d$  approaches 1, consistent with the “static” ripple discussed in the previous section.

**4.4. Peak Position,  $Z_p(t)$ , Discussion.** For the DSIMS and SNR experiments, Figures 13, 14b, and 17 all show that the position of the Ripple peak vs welding time is stationary through half the relaxation time and begins to move away from the interface only as the relaxation time is reached. This behavior is highly characteristic of reptation. The TAC model predicts that  $Z_p(t)$  is stationary initially ( $t < t_m$ ), but begins to move as the self-entanglements relax with diffusion distances on the order of the radius of gyration of the end sections,  $R_g(\text{ends})$ . The results from SNR and DSIMS on 400K materials do not show this behavior. The predictions of the PMC and Rouse models show a peak that moves continuously away from the interface with annealing time, which is again inconsistent with the experiments. The propagating peak is a result of isotropic friction and is thus expected from other tube-

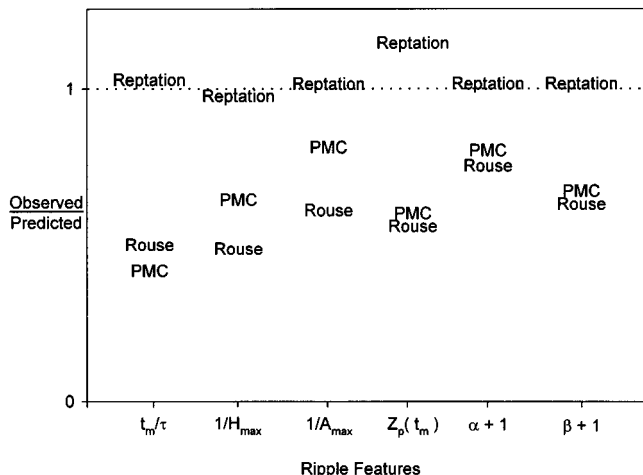


**Figure 19.** Observed/predicted ratio correlation for the Ripple characteristics, where predicted values are for one of the following models, reptation, PMC, or Rouse, as indicated. A ratio of unity implies perfect agreement between the indicated model and the experimental results.

less models as well.<sup>26–30</sup> The observed independence of the peak position on welding time provides compelling support for the reptation model.

**4.5. Dependence of Peak Position on Molecular Weight,  $Z_p(t_m, M)$ .** Peak position as a function of molecular weight from model calculations<sup>22</sup> and experimental results are plotted in Figure 18. The 400K data presented in this work extends the molecular weight range sufficiently to allow discussion of molecular weight scaling comparisons between model predictions and experiments. The peak position scales with the radius of gyration in PMC and Rouse models, and thus the predictions are  $Z_p(t_m, M) \sim M^{1/2}$ . The reptation prediction gives a peak position scaling with the tube diameter and thus  $Z_p(t_m, M) \sim M^0$ , since the tube diameter only depends on the entanglement molecular weight. The agreement of the TAC model with these results is poor. The TAC model prediction for  $Z_p(t_m, M)$  should scale with the  $R_g$  of the end labeled segment,  $R_{g(\text{ends})}$ . Since these materials are symmetrically labeled (25% of the total length is a single end section),  $R_{g(\text{ends})}$  increases with increasing molecular weight and thus a nonzero scaling with molecular weight is expected for the TAC peak position. The experimental data are only consistent with the reptation ( $d \neq 0$ ) predictions.

## 5. Summary and Conclusions

Deuterium concentration profiles were measured during welding of polystyrene HDH/DHD bilayer samples composed of oppositely labeled triblock (25–50–25) material, by dynamic secondary ion mass spectroscopy (DSIMS) and specular neutron reflectivity (SNR). Both experimental techniques measured strong depth profile ripples during welding at times less than the relaxation time and diffusion distances less than the molecular radius,  $R_g$ . The ripple shape and intensity as a function of time and molecular weight are very sensitive to the molecular dynamics controlling the interdiffusion process. By examining the experimental data, we can readily determine which dynamics model is correct and which models are inappropriate to describe microscopic details of the dynamics of highly entangled polymers.

Figure 19 shows a correlation chart for the observed/predicted ripple characteristics for the reptation, Rouse and polymer mode-coupling models. The observed/

predicted ratio is presented for the six dominant ripple characteristics, namely: (1) time at which the peak reaches a maximum,  $t_m/\tau$ ; (2) the peak maximum amplitude  $H_{\max}$ ; (3) the peak maximum area  $A_{\max}$ ; (4) the peak position at maximum amplitude  $Z_p(t_m)$ ; (5) the dependence of peak position on time,  $Z_p(t) \sim t^\alpha$ ; (6) the dependence of the peak position on molecular weight,  $Z_p(t_m, M) \sim M^\beta$ . The ripple data are normalized to unity using appropriate inverses or addition of unity where necessary, such that the ratio (observed/predicted) = 1, represents a perfect correlation or agreement between the theoretical dynamics model and the experimental data. The normalization procedure does not bias the correlation in favor of any particular model. While the quantitative values of individual ripple characteristics and their relevance to particular dynamics models has been challenged,<sup>22</sup> the correlation approach allows all of the important experimental data to be summarized, viewed at a glance, and related to the dynamics models in a more comprehensive and summary manner.

From Figure 19, it is clear that the reptation model provides the best description of the experimental data with a near-perfect correlation in all areas of the ripple characteristics. Small deviations of the reptation correlation from unity, e.g., at  $Z_p(t_m)$ , are due to the theoretical approximations used in their derivations: better agreement could be obtained if we calculated in detail the ripple profile for the HDH/DHD bilayer with regard to both Gaussian broadening of the minor chain length distribution and tube smearing of the ripple profile near the interface, as evidenced by our simulations, theoretical calculations of Grayce et al.<sup>22</sup> and previous exact minor chain calculations by Kim, Zhang, and Wool.<sup>24,42</sup> We conclude that the reptation model is the correct dynamics model to describe the microscopic details of polymer–polymer interdiffusion.

This is the first experimental method to test predictions of the polymer mode-coupling model proposed by Schweizer.<sup>19</sup> The test is particularly relevant since the Ripple experiments are new, the data did not already exist, and the nature of the experiment is very sensitive to microscopic dynamic details. We conclude that the PMC model, though highly elegant in its attempt to derive a dynamics model from first principles, is flawed with respect to its microscopic physics. Figure 19 essentially represents the results of tests to examine “tube” vs “nontube” dynamics models. The ripple features are very sensitive to the presence, or absence, of topological constraints. The reptation model makes multiple, varied, and precise quantitative predictions for the ripple features, and these are observed in explicit detail and are consistent with the concept of a chain diffusing in a tube. The PMC model utilizes an isotropic monomer friction coefficient, similar to the Rouse model, but expands the time scale for the Rouse-like motion of the monomers via coupling with the motions of all the other monomers. However, the resulting motion of the PMC chain, especially with respect to spatial distribution of monomers, is nearly identical to that of Rouse chain, as can be deduced in Figure 19. The PMC memory-integral formalism contains sufficient parameters and with the use of plausible assumptions, can describe a broad range of observed experimental data. However, the microscopic aspects of the PMC model are inconsistent with the ripple experimental data. We encourage other investigators working on melt dynamics models to interrogate their models and examine their

predictions with the range of experimental observations depicted in Figure 19.

### Closing Remarks

The reptation model was proposed by Edwards and DeGennes about 30 years ago and outlined in a seminal paper by DeGennes in 1971. The idea of a single chain diffusing in a gel provides a simple solution to a highly complex, many-bodied problem, i.e., the dynamics of polymer melts. By assuming that each chain exists in a tube formed by entanglement constraints, the complex many-chain dynamics problem was effectively replaced by a single chain, one-dimensional diffusion problem. The solution is described by,  $L^2 = 2D_1 t$ , where  $L$  is the curvilinear diffusion length of the chain along its tube axis and  $D_1 \sim 1/M$  is the one-dimensional diffusion coefficient. At the relaxation time  $\tau_d$ , the diffused length scales with the molecular weight,  $L \sim M$ . The reptation time then depends on molecular weight as  $\tau_d \sim M^3$ ; at the same time, the center of mass has moved a distance  $R_g$ , and it follows from Einstein's diffusion equation,  $R_g^2 = 2Dt_d$  that the diffusion coefficient  $D$  behaves as  $D \sim M^{-2}$ . The resulting scaling laws for the melt dynamics are readily comprehensible in terms of the tube assumption, have gained wide acceptance, and have been used by many investigators to describe a large body of experimental data. Numerous predictions for the behavior and properties of polymer fluids and solids were successfully made. Still, failure of some of these predictions, notably, the molecular weight dependence of the zero-shear melt viscosity,  $\eta \sim M^{3.4}$ , and the quest for a first-principles approach, has prompted the search for alternate models which did not, *a priori*, rely on the presence of tubes, topological constraints, and/or entanglements. We designed the Ripple test, using the HDH/DHD bilayer interdiffusion experiment, as a direct test of the microscopic details of linear polymer melt dynamics models, and we conclude that the original reptation model, as proposed by Edwards and DeGennes, is indeed correct.

**Acknowledgment.** Funding Support from NSF, Grant DMR-9596-267 is acknowledged. DSIMS was carried out at the Center for Microanalysis of Materials, University of Illinois, which is supported by the U.S. Department of Energy under grant DEFG02-91-ER45439. K.A.W. would like to thank Carlos Co for his excellent work in the development of SERF and support from the Delaware Space Grant College Fellowship Program (NASA Grant No. NGT5-40024). J.W.M. would like to thank Cambridge Isotopes for their skill in producing "halogen free" styrene- $d_8$  monomer that was essential to the synthesis of the 400K triblocks.

### References and Notes

- Wool, R. P. *Polymer Interfaces: Structure and Strength*; Hanser Publishers: Munich, Germany, 1995.
- Green, P. F.; Kramer, E. J. *Macromolecules* **1986**, *19*, 1108.
- Summerfield, G. C.; Ullman, R. *Macromolecules* **1987**, *20*, 401.
- Tirrell, M. *Rubber Chem. Technol.* **1984**, *57*, 523.
- Klein, J.; Briscoe, B. *J. Proc. R. Soc. London, A* **1979**, *365*, 53.
- Agrawal, G.; Wool, R. P.; Dozier, W. D.; Felcher, G. P.; Zhou, J.; Pispas, S.; Mays, J. W.; Russell, T. P. *J. Polym. Sci., Part B* **1996**, *34*, 2919.
- Russell, T. P.; Deline, V. R.; Dozier, W. D.; Felcher, G. P.; Agrawal, G.; Wool, R. P.; Mays, J. W. *Nature* **1993**, *365*, 235.
- Agrawal, G.; Wool, R. P.; Dozier, W. D.; Felcher, G. P.; Russell, T. P.; Mays, J. W. *Macromolecules* **1994**, *27*, 4407.
- Russell, T. P. *Mater. Sci. Rep.* **1990**, *5*, 171.
- Lekner, J. *Theory of Reflection*; Martinus Nijhoff Publishers: Boston, MA, 1987.
- Stamm, M. *Reflection of Neutrons for the Investigation of Polymer Interdiffusion at Interfaces*. In *Physics of Polymer Surfaces and Interfaces*; Sanchez, I. C., Ed.; Butterworth-Heinemann: Boston, MA, 1992; p 163.
- Parratt, L. G. *Phys. Rev.* **1954**, *95*, 359.
- Co, C.; Welp, K. A. Improved Reflectivity Fitting Using SERF (Spreadsheet Environment Reflectivity Fitting): NOBUGS; Argonne National Labs, Argonne, IL, 1998; Welp, K. A.; Co, C.; Wool, R. P. Submitted for publication in *Rev. Sci. Instrum.*
- Whitlow, S. J.; Wool, R. P. *Macromolecules* **1989**, *22*, 2648.
- Whitlow, S. J.; Wool, R. P. *Macromolecules* **1991**, *24*, 5926.
- Garbassi, F.; Morra, M.; Occhiello, E. *Polymer Surfaces: From Physics to Technology*; John Wiley: New York, 1994.
- Benninghoven, A.; Rudenaur, F. G.; Werner, H. W. *Secondary Ion Mass Spectrometry*; John Wiley: New York, 1987; Vol. 86.
- Rouse, P. E. *J. Chem. Phys.* **1953**, *21*, 1272.
- Schweizer, K. S. *J. Chem. Phys.* **1989**, *91*, 5822.
- De Gennes, P. G. *J. Chem. Phys.* **1971**, *55*, 572.
- Doi, M.; Edwards, S. F. *The Theory of Polymer Dynamics*; Oxford University Press: New York, 1986.
- Grayce, C. J.; Szamel, G.; Schweizer, K. S. *J. Chem. Phys.* **1995**, *102*, 2222.
- Welp, K. A.; Sokol, K.; Wool, R. P. Work in progress, 1998.
- Kim, Y. H.; Wool, R. P. *Macromolecules* **1983**, *16*, 1115.
- Lodge, T. P.; Rotstein, N. A.; Prager, S. *Adv. Chem. Phys.* **1990**, *129*, 1.
- Skolnick, J.; Kolinski, A. *Adv. Chem. Phys.* **1990**, *78*, 223.
- Ngai, K. L. *Comments Solid State Phys.* **1979**, *9*, 1651.
- McKenna, G. B.; Ngai, K. L.; Plazek, D. J. *J. Polym.* **1985**, *26*, 1653.
- Herman, M. F. *Macromolecules* **1992**, *25*, 4931.
- Herman, M. F. *Macromolecules* **1992**, *25*, 4925.
- Hess, W. *Macromolecules* **1988**, *21*, 2620.
- Kavassalis, T. A.; Noolandi, J. *Macromolecules* **1988**, *21*, 2869.
- Fixman, M. *J. Chem. Phys.* **1988**, *89*, 3892.
- Fixman, M. *J. Chem. Phys.* **1988**, *89*, 3912.
- Doi, M. *J. Polym. Sci.: Polym. Lett. Ed.* **1981**, *19*, 265.
- Doi, M. *J. Polym. Sci.: Polym. Phys. Ed.* **1983**, *21*, 667.
- Daoud, M.; Gennes, P. G. *J. Polym. Sci.: Polym. Phys. Ed.* **1979**, *17*, 1971.
- des Cloizeaux, J. *Europhys. Lett.* **1988**, *5*, 437.
- des Cloizeaux, J. *Macromolecules* **1990**, *23*, 4678.
- Graessley, W. W. *Adv. Polym. Sci.* **1982**, *47*, 68.
- Russell, T. P., Personal communication.
- Zhang, H.; Wool, R. P. *Macromolecules* **1989**, *22*, 3018.

MA971692N